Journal of Experimental and Theoretical Physics, Vol. 101, No. 5, 2005, pp. 844–855.
Translated from Zhurnal Éksperimental'noĭ i Teoreticheskoĭ Fiziki, Vol. 128, No. 5, 2005, pp. 974–986.

ORDER, DISORDER, AND PHASE TRANSITIONS IN CONDENSED SYSTEMS

Effective Hamiltonian for HTSC Cuprates Taking into Account Electron–Phonon Interaction in the Strong-Correlation Regime

S. G. Ovchinnikov and E. I. Shneĭder

Kirenskiĭ Institute of Physics, Siberian Division, Russian Academy of Sciences, Akademgorodok, Krasnoyarsk, 660036 Russia

e-mail: shneyder@iph.krasn.ru

Received April 18, 2005

Abstract—Electron–phonon interaction is sequentially derived from a realistic *p–d* multiband model for the cuprates under conditions of strong electron correlations. The electronic structure is described using the representation of the Hubbard *X* operators in a generalized tight-binding method. Dependences of the diagonal and off-diagonal (on lattice sites) matrix elements of electron–phonon interaction on the wavevectors are found for three phonon modes, namely, breathing, apical breathing, and bending modes. The interactions of the breathing and bending modes with electrons are shown to contribute to the formation of kinks in the (0; 0)–(π; π) and (0; 0)–(π; 0) directions, respectively. A low-energy *t–J** model with phonons is developed; apart from electron–phonon interaction, it also includes spin–phonon interaction. The elimination of phonons gives an effective electron–electron interaction that depends on the occupation number of a multielectron term and on the carrier concentration due to strong electron correlations. © *2005 Pleiades Publishing, Inc.*

1. INTRODUCTION

Despite significant progress reached in studying high-temperature superconductivity (HTSC) in layered cuprates, the HTSC mechanism is still unclear. Among numerous mechanisms proposed in the initial stage of investigating HTSC, the following two mechanisms have been most often discussed recently: the traditional mechanism of electron–phonon interaction (EPI) and the spin-fluctuation mechanism [1]. The latter is known to be caused by strong electron correlations that result in a long-range antiferromagnetic (AFM) order in undoped dielectric cuprates and to a short-range AFM order in weakly doped cuprates. Interest in electron–phonon interaction, which is present in all substances and can be strong in layered cuprates due to specific features of their crystal structure, has currently quickened because of inflection points (kinks) detected in electron dispersion laws in ARPES (angle-resolved photoemission spectroscopy) measurements [2]. Note that kinks were found in many hole cuprates, but they are absent in the electron cuprates with a *T*' structure ($Nd_{2-x}Ce_xCuO_4$). The kink energy measured from the Fermi level ($\omega_k \approx 70$ meV) is virtually universal, and the effect is most pronounced in the form of a bend in the dispersion law in the diagonal direction $\Gamma \longrightarrow M$, (0; 0)–(π; π) of the Brillouin zone. A kink at an energy $\omega_k \approx 40$ meV was also detected in the vicinity of the *X*((π; 0), (0; π)) and Bi2212 points [3], and it increases sharply as the temperature decreases below T_c (see the review of ARPES data in [4]). The nature of the kink is obviously related to electron–boson interaction; however, the question of what bosons, namely, phonons or spin fluctuations, are responsible for these renormalizations of an electronic spectrum near the Fermi level is a matter of dispute [5]. The kink can result from interaction with optical phonons [6] or with spin fluctuations [7, 8].

Thus, to describe both superconducting pairing and the properties of the normal state in the cuprates, one has to take into account the interactions of electrons with phonons and spin fluctuations. To describe optimally or strongly doped compositions, one can start from ordinary band theory; however, to discuss the entire phase diagram of cuprates, beginning from undoped antiferromagnetic dielectrics, one has to describe electrons in the strong-correlation regime. Various modifications of the one- and multiband Hubbard models led to a low-energy effective *t–J* model that describes electron interaction with spin fluctuations in the Hubbard bands [9, 10]. However, electron–phonon interaction in the strong-correlation regime has been studied to a lesser extent (see recent review [11]). As a rule, researchers consider the *t–J* model with local interaction of electrons with a certain optical mode. At the same time, to discuss the symmetry of the superconducting state and the differences in kinks located in different regions of the Brillouin zone, it is necessary to know an explicit dependence of the matrix elements $g^{(\nu)}(\mathbf{k}, \mathbf{q})$ of electron–phonon interaction on the incoming momentum **k** transferred by **q** and the number ν of the phonon mode. The purpose of this work is to sequentially derive electron–phonon interaction from a

realistic *p–d* multiband model for cuprates in the strong-correlation regime [12] and to realistically describe the phonons that interact most strongly with electrons.

In the general case, we can distinguish diagonal and off-diagonal contributions to the electron–phonon interaction in the nodal representation. Strong electron correlations and the diagonal electron–phonon interaction were simultaneously taken into account in [13–17]. It was found that the following three phonon modes interact most strongly with electrons: the longitudinal breathing mode (oxygen-ion vibrations in the CuO_2 plane that deform the Cu–O bond), the apical breathing mode (vibrations of apical oxygen ions that deform the Cu–O bond along the *c* axis), and the bending mode (oxygen-ion vibrations in the CuO_2 layer normal to the Cu–O bond) (Fig. 1). Neutron-scattering experiments revealed the maximum softening of the breathing mode at the boundary of the Brillouin zone, at the $(\pi/a; 0; 0)$ point [18, 19]. The joint effect of EPI and spin-fluctuation interaction on the superconducting pairing without regard for strong electron correlations was analyzed in [20]. As follows from the results of all these works, the breathing mode interacts most strongly at a phonon quasi-momentum $\mathbf{q} \sim \mathbf{Q} = (\pi/a; \pi/a)$ and breaks pairing with the $d_{x^2-y^2}$ symmetry; the bending mode has maximum interaction at small $\mathbf{q}$; and the apical breathing mode has a matrix interaction element that is independent of the in-plane wavevector $\mathbf{q}$. Oxygen-ion vibrations normal to the CuO_2 plane strongly modulate the ionic component of the chemical bond in the cuprates by changing the Madelung potential; hence, they strongly interact with electrons [11].

Kinks in ARPES experiments at the nodal ($\mathbf{k} = (\pi/2a; \pi/2a)$) and antinodal ($\mathbf{k} = (\pi/a; 0)$) points have different boson frequencies and different temperature dependences; therefore, their analysis requires a detailed description of EPI, in particular, the description of the dependence of the matrix elements $g^{(\nu)}(\mathbf{k}, \mathbf{q})$ on not only the transferred momentum $\mathbf{q}$ but also on the incoming momentum $\mathbf{k}$ [21]. The latter dependence can only be caused by the off-diagonal part of EPI. When the authors of [22, 23] derived EPI, they took into account strong electron correlations within the framework of the three-band *p–d* model and diagonal and off-diagonal EPIs and only considered the breathing mode. As a result, they constructed an effective *t–J* model with EPI. In this work, we investigate the interaction of strongly correlated electrons with all three modes given above and find diagonal and off-diagonal contributions to EPI. By comparing the crystal structures and phonon spectra of LSCO (*T* structure) and NCCO (*T*' structure), we could reveal the contributions to EPI that disappear when passing from the *T* to the *T*' structure and could explain why the EPI in the *T*' structure is significantly weaker than that in the hole cuprates.

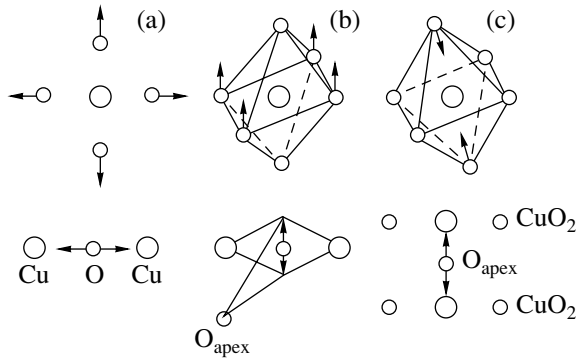

Fig. 1. Schematic diagram for atomic displacements for (a) the breathing mode, (b) the bending mode, and (c) the apical breathing mode.

2. DERIVATION OF ELECTRON–PHONON INTERACTION USING A MULTIBAND *p–d* MODEL FOR LAYERED CUPRATES

The Hamiltonian of the CuO_2 layer in the multiband *p–d* model can be written as follows (in the hole representation) [24]:

$$H_{pd} = \sum_{i\lambda\sigma}(\varepsilon_{i\lambda} - \mu)n_{i\lambda\sigma} + \sum_{ij\sigma}\sum_{\lambda\lambda'} t_{ij}^{\lambda\lambda'} a_{i\lambda\sigma}^{\dagger} a_{j\lambda'\sigma} + \sum_{ij\sigma\sigma'}\sum_{\lambda\lambda'}(V_{ij}^{\lambda\lambda'} n_{i\lambda\sigma} n_{j\lambda'\sigma'} - J_{ij}^{\lambda\lambda'} a_{i\lambda\sigma}^{\dagger} a_{i\lambda\sigma'} a_{j\lambda'\sigma'}^{\dagger} a_{j\lambda'\sigma}). \quad (1)$$

Here, $n_{i\lambda\sigma} = a_{i\lambda\sigma}^{\dagger} a_{j\lambda\sigma}$, $a_{i\lambda\sigma}^{\dagger}$ is the operator of production of a hole on the site $i \equiv R_i$ in the orbital state λ with the spin projection σ and the energy $\varepsilon_{i\lambda}$; μ is the chemical potential; $t_{ij}^{\lambda\lambda'}$ is the matrix element of an atomic jump; and $V_{ij}^{\lambda\lambda'}$ and $J_{ij}^{\lambda\lambda'}$ are the matrix elements of the Coulomb and exchange interactions, respectively. Unlike the three-band *p–d* model [25, 26], the multiband model takes into account both the $d_{x^2-y^2}$ and $d_{3z^2-r^2} \equiv d_{z^2}$ copper orbitals (although the other three t_{2g} orbitals can also be included, they are filled by electrons and their energy levels in the electron valence band are well below the low-energy range ($E \le 1$ eV) to be studied here). For oxygen ions lying in the CuO_2 layer, we take into account the p_x and p_y orbitals, and the p_z orbitals of the apical oxygen (which are present in the *T* structure and are absent in the *T*' structure) are also considered. Important microscopic model parameters are the following: t_{pd} is a hopping between the $d_{x^2-y^2}$ copper and the in-plane oxygen; t_{pp} is a hopping between neighbor-

ing (O_x and O_y) oxygen ions; and t'_{pd} and t'_{pp} are hoppings between copper and the apical oxygen and the in-plane and apical oxygen, respectively. From the Coulomb interactions, we distinguish the intra-atomic interactions of two holes in one (U_d is the Hubbard parameter) and different (V_d) orbitals, the corresponding interactions (U_p and V_p) for oxygen, the Coulomb interaction of neighboring copper and oxygen (V_{pd}), and the interaction of neighboring oxygen ions (V_{pp}). From the exchange interactions, we distinguish intra-atomic (Hund) exchange parameters J_d and J_p. A detailed analysis of Hamiltonian (1) and various matrix elements, as well as a procedure for the calculation of the band structure of quasiparticles with allowance for strong electron correlations using a generalized tight-binding (GTB) method, are given in [12, 27].

After the Wannier functions have been constructed in the framework of the GTB method, Hamiltonian (1) is written as the sum of intracell (H_c) and intercell (H_{cc}) parts [12, 27]

$$H = H_c + H_{cc},$$

$$H_c = \sum_f H_f, \quad H_f = H_f^{(b)} + H_f^{(a)} + H_f^{(ab)}, \qquad (2)$$

$$H_{cc} = \sum_{fg\sigma} (h_{fg}^{(b)} + h_{fg}^{(a)} + h_{fg}^{(ab)}).$$

Here, the f and g sites are only related to the copper sublattice (the cell is the CuO_6 or CuO_4 cluster), since the Wannier functions are centered at the Cu sites. The superscripts a and b indicate the symmetries of the Wannier functions: the $d_{x^2-y^2}$ copper states are hybridized inside the cell with the molecular b_{1g} orbital of the in-plane oxygen, and the d_{z^2} copper states are hybridized with the a_{1g} states of the in-plane oxygen and the p_z states of the apical oxygen. Apart from one-particle p–d and p–p hoppings inside the cell, the $H_f^{(b)}$ and $H_f^{(a)}$ Hamiltonians contain intracell Coulomb interactions. For example, U_p and V_{pd} are involved in all three H_f terms. However, $H_f^{(ab)}$ only contains Coulomb and exchange interactions, since the Wannier functions inside the cell are orthogonal. They are mixed due to hoppings between neighboring cells, and this mixing is contained in the $h_{fg}^{(ab)}$ term.

To take into account strong electron correlations within the framework of the GTB method, we first exactly diagonalize the H_f Hamiltonian and use its complete set of eigenstates $\{|p\rangle\}$ to construct the Hubbard X operators $X_f^{pq} \equiv |p\rangle\langle q|$. In the second stage, the intercell Hamiltonian part H_{cc} is written in the X representation, and it has the same operator structure ($\sim t_{fg} X_f X_g$) as the hopping Hamiltonian in the standard Hubbard model. This fact allows us to find the Green function and a band structure using perturbation theory. A dispersion equation for the calculation of a band structure in the GTB method has the form (in the paramagnetic phase)

$$\det \left\| \frac{E - \Omega_m}{F_m} \delta_{mm'} - \sum_{\lambda\lambda'} \gamma_{\lambda\sigma}(m) T_{\lambda\lambda'}(k) \gamma_{\lambda'\sigma}(m') \right\| = 0, \qquad (3)$$

where the coefficients $\gamma_{\lambda\sigma}(m)$ of the representation of the one-electron operators in terms of the Hubbard X operators,

$$a_{f\lambda\sigma} = \sum_m \gamma_{\lambda\sigma}(m) X_f^m, \quad m \longleftrightarrow (p, q), \qquad (4)$$

are calculated after the exact diagonalization of H_f. The Ω_m energies have a one-particle meaning, and they are defined as resonances between multielectron terms $|p\rangle$ and $|q\rangle$: $\Omega_m = E_p - E_q$. The filling factors $F_m = \langle X^{pp} \rangle + \langle X^{qq} \rangle$, just like the Ω_m energies, are calculated after the exact diagonalization of H_f. Finally, the intercell hopping matrix elements $T_{\lambda\lambda'}(k)$ are defined by different p–d and p–p hoppings. For example, electron production at the bottom of the conduction band of undoped La_2CuO_4 or Nd_2CuO_4 is related to a resonance between the vacuum ($|0\rangle$, the $d^{10}p^6$ configuration) molecular orbitals and the one-hole ($|\sigma\rangle$, $\sigma = \pm 1/2$; a mixture of the d^9p^6 and $d^{10}p^5$ configurations) molecular orbitals. Hole production near the valence band top is related to resonances Ω_S between the one-hole $|\sigma\rangle$ states and the two-hole $|s\rangle$ ^1A singlet that is mixed with the band of triplet excitations Ω_T ($|1, \sigma\rangle \longrightarrow |2, T\rangle$) with the participation of the two-hole ^3B triplet.

In the one-hole sector of the Hilbert space, the blocks of the H_f matrix with the b and a symmetries have the form

$$H_f^{(b)} = \begin{pmatrix} \varepsilon(d_{x^2-y^2}) & -\tau_b \\ -\tau_b & \varepsilon_b \end{pmatrix}, \qquad (5)$$

$$H_f^{(a)} = \begin{pmatrix} \varepsilon(d_{z^2}) & -\tau_a & -\tau'_{pd} \\ -\tau_a & \varepsilon_a & -t'_{pp} \\ -\tau'_{pd} & -t'_{pp} & \varepsilon(p_z) \end{pmatrix}, \qquad (6)$$

where the hopping parameters τ and the energies of the oxygen b and a orbitals are renormalized as compared to the initial atomic values due to the construction of the Wannier functions. The corresponding matrices in the two-hole sector have a large dimension; they are given in an explicit form in [12, 27] and are not discussed here.

After diagonalizing the intracell H_c part and after passing to the X-operator representation, we can write electron Hamiltonian (1) as

$$H_{\rm el} = \sum_{fn\gamma}(E_{n\gamma} - n\mu)X_f^{n\gamma,\,n\gamma} + \sum_{fg}\sum_{mm'} t_{fg}^{mm'} X_f^{\dagger m} X_g^{m'}. \quad (7)$$

At low energies near the bottom of the conduction band and the top of the valence band, we restrict ourselves to the following set of $|n\gamma\rangle$ terms: $n = 0$, $|0\rangle$; $n = 1$, $|\sigma\rangle$, $\sigma = \pm 1/2$; $n = 2$, singlet $|s\rangle$ and triplet $|T, M\rangle$, $M = 0, \pm 1$ [12]. Indices m, m' denote various hole excitations. For this set of $|n\gamma\rangle$ terms, the disappearance of a hole with a spin σ in Eq. (4) is described by the following quasiparticles: at $m = 0$, $(0, \sigma)$; at $m = 1$, $(\bar{\sigma}, s)$; at $m = 2$, $(\bar{\sigma}, T0)$; and at $m = 3$, $(\sigma, T2\sigma)$.

As usual, when EPI is derived in terms of the GTB method, it is necessary to take into account the modulation of the intra-atomic ($\varepsilon_{i\lambda}$) and interatomic ($t_{ij}^{\lambda\lambda'}$) parameters upon atomic displacements. Moreover, in our case, EPI is contributed by the modulation of the Coulomb interatomic interaction. It is important that the modulation of the one- and two-particle Hamiltonian parameters due to atomic displacements contributes to not only the one-particle but also the two-particle terms; in the general case, it also contributes to the multiparticle terms $E_{n\gamma}$ (where n is the number of electrons, and γ is the set of quantum numbers) that determine the resonance energies Ω in Eq. (3), whence a diagonal contribution to EPI appears. The modulation of various atomic-jump and Coulomb-interaction parameters also causes an off-diagonal contribution to EPI. As a result of atomic displacements, the energies of the $|n\gamma\rangle$ terms become site-dependent:

$$E_{n\gamma}(\mathbf{R}_i) = E_{n\gamma}(\mathbf{R}_{i0} + \mathbf{u}_i) = E_{n\gamma}(0) + \mathbf{g}_{n\gamma}\mathbf{u}_i. \quad (8)$$

Similarly, the hopping and interaction parameters depend on the difference in the sites $\mathbf{R}_i - \mathbf{R}_j = \mathbf{R}_{i0} - \mathbf{R}_{j0} + \mathbf{u}_{ij}$, $\mathbf{u}_{ij} = \mathbf{u}_i - \mathbf{u}_j$. In a linear approximation, we have

$$t_{fg}^{mm'} = t_{fg}^{mm'}(0) + \mathbf{V}^{mm'} \cdot \mathbf{u}_{fg}. \quad (9)$$

Here, a set of the phenomenological $\mathbf{g}_{n\gamma}$ and $\mathbf{V}^{mm'}$ parameters specifies the diagonal and off-diagonal contributions to EPI. As a result, we obtain electron Hamiltonian (7), in which all energies belong to the undisturbed lattice (i.e., $E_{n\gamma}(0)$ and $t_{fg}(0)$), and the EPI Hamiltonian

$$H_{\rm el-ph} = \sum_{fn\gamma}\mathbf{g}_{n\gamma}\cdot\mathbf{u}_f X_f^{n\gamma,\,n\gamma} + \sum_{fg}\sum_{mm'}\mathbf{V}^{mm'}\cdot\mathbf{u}_{fg}X_f^{\dagger m}X_g^{m'} \quad (10)$$

in the system of strongly correlated electrons.

Using the breathing mode as an example, we consider characteristic displacements and modulation of the corresponding Hamiltonian parameters. Figure 1 shows a fragment of the CuO_2 layer and the directions of oxygen-ion displacements for the three phonon modes under discussion. For the breathing mode, a displacement of the O^{2-} ion along the Cu–O bond (Fig. 1a) changes the Madelung potential and, thus, the d-level energy in the crystal field:

$$\varepsilon_i(d_{x^2-y^2}) = \varepsilon_{d0} + \mathbf{g}\cdot\mathbf{u}_i,$$

$$\mathbf{u}_i = u_x\left(R_i + \frac{a_x}{2}\right) - u_x\left(R_i - \frac{a_x}{2}\right) + u_y\left(R_i + \frac{a_y}{2}\right) - u_y\left(R_i - \frac{a_y}{2}\right). \quad (11)$$

In the approximation that is linear in displacements, modulation of the ε_p level on oxygen is absent because of the symmetry, since the contributions from the left and right copper ions are canceled (Fig. 1a). As a result, we have modulation of the charge transfer energy: $\Delta_i = \varepsilon_p - \varepsilon_i(d_{x^2-y^2}) = \Delta_0 - \mathbf{g}\cdot\mathbf{u}_i$. Analogous linear-in-displacement contributions appear in the parameters of hoppings between copper and the in-plane oxygen ($t_{pd}(i) = t_{pd}(0) + \delta t_{pd}$), between oxygen and the oxygen inside the CuO_2 layer ($t_{pp}(i) = t_{pp}(0) + \delta t_{pp}$), and between the apical oxygen and the in-plane oxygen ($t'_{pp}(i) = t'_{pp}(0) + \delta t'_{pp}$); they also appear in the parameters of the Coulomb interaction of copper with oxygen ($V_{pd}(i) = V_{pd}(0) + \delta V_{pd}$) and of oxygen with oxygen ($V_{pp}(i) = V_{pp}(0) + \delta V_{pp}$).

In [12], the parameters of Hamiltonian (1) were considered as phenomenological and were found from a comparison with ARPES experimental data for undoped $Sr_2CuO_2Cl_2$ oxychlorides. These parameters have recently been calculated using the LDA and LSD + U band-theory methods [28]. All hopping integrals were found to be of the same order of magnitude: $t_{pp} \approx t'_{pp} \approx 0.4$–$0.5t_{pd}$. The displacement dependence of the parameters has not been calculated; therefore, in this work we cannot describe EPI without using fitting parameters. The modulation corrections to the hopping integrals are assumed to be of the same order of magnitude: $\delta t_{pd} \sim \delta t_{pp} \sim \delta t'_{pp} \sim \delta t'_{pd}$.

Apart from the modulation of the Coulomb interactions and the crystal field, all these linear-in-displacement modulations renormalize the energies of the one-hole b_{1g} doublet $|\sigma\rangle$ and the two-hole ^1A singlet and ^3B triplet, which results in the modulation of the Ω_S and Ω_T energies (diagonal contribution to EPI). The off-diagonal contribution results from the modulation of $T_{\lambda\lambda'}$ in dispersion equation (3). Since the distance depen-

dences of all matrix elements of Hamiltonian (1) are unknown, we introduce two parameters of the diagonal and off-diagonal EPIs for each electron band and each phonon mode (ν). Using the completeness condition

$$X_f^{0,0} + \sum_\sigma X_f^{\sigma,\sigma} + X_f^{S,S} + \sum_{M=-1}^{1} X_f^{TM,TM} = 1 \qquad (12)$$

for the multielectron basis of the cell, we can eliminate one parameter of the diagonal EPI and write

$$H_{\text{dia}}^{(\nu)} = \sum_f \mathbf{u}_{f,\nu} \times \left[\sum_\sigma \mathbf{g}_\sigma^{(\nu)} X_f^{\sigma\sigma} + \mathbf{g}_S^{(\nu)} X_f^{SS} + \sum_M \mathbf{g}_T^{(\nu)} X_f^{TM,TM} \right]. \qquad (13)$$

As usual, the displacement vector is represented in the form

$$\mathbf{u}_{f,\nu} = \frac{1}{\sqrt{N}} \sum_{\mathbf{q},\alpha} \frac{\mathbf{e}_{\alpha,\nu}}{\sqrt{2M_\alpha \omega_{\mathbf{q},\nu}}} \varphi_{\mathbf{q},\nu} \exp(i\mathbf{q}(\mathbf{R}_f + \mathbf{R}_\alpha)), \qquad (14)$$

where M_α is the ion α mass, $\mathbf{R}_\alpha$ is the ion radius vector in the $\mathbf{R}_f$ cell, $\mathbf{e}_{\alpha,\nu}$ is the polarization vector, and $\varphi_{\mathbf{q},\nu} = b_{\mathbf{q},\nu} + b^\dagger_{-\mathbf{q},\nu}$ and $b_{\mathbf{q},\nu}(b^\dagger_{-\mathbf{q},\nu})$ are operators of annihilation (production) of phonon ν with the $\mathbf{q}$ wavevector. Neglecting the copper-ion displacements (which are small as compared to the oxygen-ion displacements), for the breathing optical mode (ν = 1) we find

$$\mathbf{u}_{f,1} = \frac{2i}{\sqrt{2M_O N}} \sum_{\mathbf{q}} \frac{\varphi_{\mathbf{q},1}}{\sqrt{\omega_{\mathbf{q},1}}} e^{i\mathbf{q}\cdot\mathbf{R}_f} \times \left[e_x(O_x) \sin\frac{q_x a}{2} + e_y(O_y) \sin\frac{q_y a}{2} \right]. \qquad (15)$$

As a result, the diagonal part of EPI for the ν mode can finally be written as

$$H_{\text{dia}}^{(\nu)} = \frac{1}{\sqrt{N}} \sum_{\mathbf{kq}\nu} \sum_m g_{\text{dia},m}^{(\nu)}(\mathbf{q}) X^{\dagger m}_{\mathbf{k}+\mathbf{q}} X^m_{\mathbf{k}} \varphi_{\mathbf{q},\nu}, \qquad (16)$$

where for the breathing mode we have

$$g_{\text{dia},m}^{(1)}(\mathbf{q}) = \frac{2ig_m^{(1)}}{\sqrt{2M_O\omega_{\mathbf{q},1}}} \times \left[e_x(O_x) \sin\frac{q_x a}{2} + e_y(O_y) \sin\frac{q_y a}{2} \right]. \qquad (17)$$

The off-diagonal part of EPI for this mode is

$$H_{\text{off}}^{(1)} = \sum_{fg} \sum_{mm'} \mathbf{V}_{mm'}^{(1)} \cdot (\mathbf{u}_{f,1} + \mathbf{u}_{g,1}) X_f^{\dagger m} X_g^{m'} \qquad (18)$$

and can be represented as

$$H_{\text{off}}^{(\nu)} = \frac{1}{\sqrt{N}} \sum_{\mathbf{kq}\nu} \sum_{mm'} g_{\text{off},mm'}^{(\nu)}(\mathbf{k},\mathbf{q}) X^{\dagger m}_{\mathbf{k}+\mathbf{q}} X^{m'}_{\mathbf{k}} \varphi_{\mathbf{q},\nu}, \qquad (19)$$

where

$$g_{\text{off},mm'}^{(1)}(\mathbf{k},\mathbf{q}) = \frac{8i\mathbf{V}_{mm'}^{(1)}}{\sqrt{2M_O\omega_{\mathbf{q},1}}} \times \left[e_x(O_x) \sin\frac{q_x a}{2} + e_y(O_y) \sin\frac{q_y a}{2} \right] \times [\gamma(\mathbf{k}) + \gamma(\mathbf{k}+\mathbf{q})] \qquad (20)$$

and $\gamma(\mathbf{q}) = (\cos q_x a + \cos q_y a)/2$.

For the apical breathing mode (ν = 2), the displacements of the apical oxygen ions along the *z* axis modulate the crystal field on copper and, thus, $\delta\varepsilon_d$, the Cu–O_{ap} bond length, the $\delta t'_{pd}$ hoppings, and the $\delta t'_{pp}$ hoppings between the apical and in-plane oxygen (Fig. 1b). All these effects contribute only to the diagonal EPI, since they change the parameters only inside the $\mathbf{R}_f$ cell. Of course coupling between neighboring CuO_2 layers also appear; however, we restrict ourselves to only one-layer cuprates in this work. Strong EPI for this mode and its doping-induced softening were predicted in [29].

For a two-dimensional vector $\mathbf{q} = (q_x, q_y)$, we have $\mathbf{q}\cdot\mathbf{R}_a = 0$; therefore, we can write

$$\mathbf{u}_{f,2} = \frac{1}{\sqrt{N}} \sum_{\mathbf{q}} \frac{e_z(O_{\text{ap}})}{\sqrt{2M_O\omega_{\mathbf{q},2}}} \varphi_{\mathbf{q},2} e^{i\mathbf{q}\cdot\mathbf{R}_f}, \qquad (21)$$

so that

$$g_{\text{dia},m}^{(2)}(\mathbf{q}) = \frac{\mathbf{g}_m^{(2)}}{\sqrt{2M_O\omega_{\mathbf{q},2}}} e_z(O_{\text{ap}}) \qquad (22)$$

depends only weakly on $\mathbf{q}$ through the $\omega_{\mathbf{q},2}$ dispersion. The off-diagonal part of EPI for the apical breathing mode is absent:

$$g_{\text{off}}^{(2)}(\mathbf{k},\mathbf{q}) = 0. \qquad (23)$$

For the bending mode (ν = 3), displacements in the tetragonal phase are transverse to the Cu–O bond (Fig. 1c), and the microscopic nature of EPI for this mode is not so obvious. Indeed, because of the symmetry, the Cu–O bond lengths, the crystal field, and the t_{pd} hopping cannot be modulated in the linear-in-displacement approximation; their modulations are proportional to the displacement squared [13]. Linear contributions appear only in the corrugated CuO_2 layer owing to orthorhombic distortions, and they are small due to

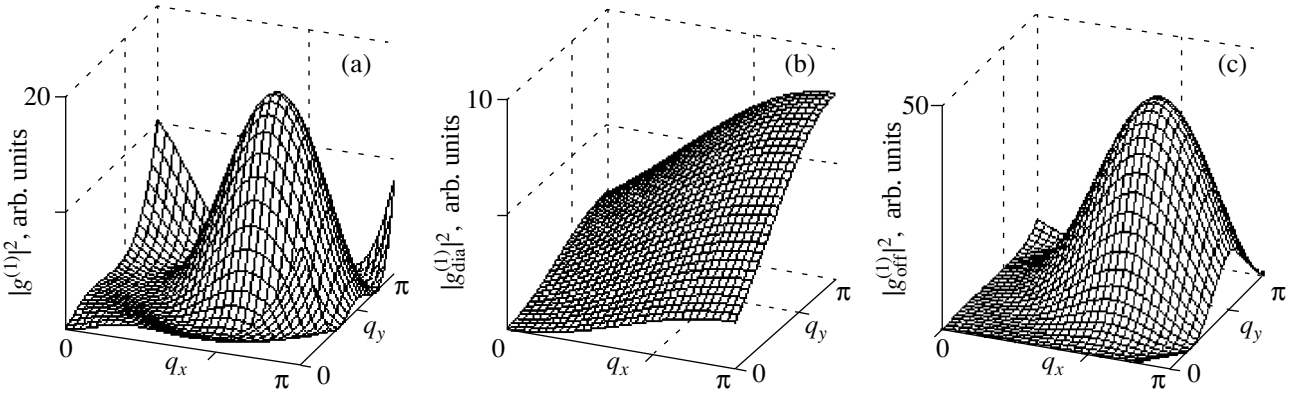

Fig. 2. EPI matrix element for the breathing mode at the $\mathbf{k}_n$ nodal point: (a) the total element, (b) the diagonal part, and (c) the off-diagonal part.

the small angle of corrugation. It should be noted that, in [13] and most related works, EPI is derived from an analysis of displacements using a simplified Hubbard model or the three-band *p–d* model with absent apical-oxygen states. In our *p–d* multiband model, the presence of the apical oxygen leads to the modulation of the distance between the in-plane and apical oxygen (Fig. 1c). As a result, the $\delta t'_{pp}$ and $\delta V'_{pp}$ parameters are modulated in the linear-in-displacement approximation. Moreover, for this mode, the modulation of the Madelung potential (the ionic component of the chemical bond) contributes significantly to EPI [11], since oxygen-ion vibrations transversely to the CuO_2 plane are weakly shielded.

Finally, the diagonal EPI with the bending mode can be written in the form of Eq. (16) with the matrix element

$$g^{(3)}_{\text{dia},\,m}(\mathbf{q}) = \frac{2\mathbf{g}^{(3)}_m}{\sqrt{2M_O\omega_{\mathbf{q},\,3}}} \times\left[e_z(O_x)\cos\frac{q_x a}{2} + \mathrm{e}_z(O_y)\cos\frac{q_y a}{2}\right]. \tag{24}$$

The matrix element of the off-diagonal EPI with the same mode is

$$g^{(3)}_{\text{off},\,mm'}(\mathbf{k},\mathbf{q}) = \frac{2\mathbf{V}^{(3)}_{mm'}}{\sqrt{2M_O\omega_{\mathbf{q},\,3}}} \times\left[e_z(O_x)\cos\left(k_x+\frac{q_x}{2}\right)a + \mathrm{e}_z(O_y)\cos\left(k_y+\frac{q_x}{2}\right)a\right]. \tag{25}$$

By summarizing the results of this section, we write the EPI Hamiltonian as

$$H_{\text{el–ph}} = \sum_{\mathbf{k}\mathbf{q}\nu}\sum_{mm'} g^{(\nu)}_{mm'}(\mathbf{k},\mathbf{q})X^{\dagger m}_{\mathbf{k}+\mathbf{q}}X^{m'}_{\mathbf{k}}(b_{\mathbf{q},\,\nu}+b^{\dagger}_{-\mathbf{q},\,\nu}), \tag{26}$$

$$g^{(\nu)}_{mm'}(\mathbf{k},\mathbf{q}) = \delta_{mm'}g^{(\nu)}_{\text{dia},\,m}(\mathbf{q}) + g^{(\nu)}_{\text{off},\,mm'}(\mathbf{k},\mathbf{q}).$$

The g_{dia} and g_{off} matrix elements for the three phonon modes under study are given by Eqs. (17), (20), (22)–(25).

It should be noted that the introduction of two phenomenological parameters ($\mathbf{g}^{(\nu)}_m$ and $\mathbf{V}^{(\nu)}_{mm'}$) for the diagonal and off-diagonal EPIs for each mode is related to not only a large amount of different microscopic contributions but also to incomplete knowledge of the distance dependences of various parameters. For example, even for the simplest particular case of EPI in the *t–J* model with the breathing mode, two works ([22, 23]) solving similar problems give different results: a large diagonal contribution (~0.25 eV) and a two orders of magnitude smaller off-diagonal contribution in [22] in contrast to virtually the same (~0.03 eV) diagonal and off-diagonal contributions to EPI in [23]. When several EPI mechanisms are taken into account, different contributions begin to interfere; for instance, the contribution of δV_{pd} decreases the contribution of δt_{pd} by approximately 30% [22]. When passing to a realistic model with a large number of contributions to EPI, the estimation errors of matrix elements accumulate; therefore, we think that the decision to restrict ourselves to phenomenological parameters was reasonable.

3. ANALYSIS OF THE SYMMETRY OF ELECTRON–PHONON INTERACTION

It is convenient to consider the dependences of the matrix elements on **k** and **q**, which were obtained by analyzing the atomic displacements in each mode, using maps in which $|g^{(\nu)}(\mathbf{k},\mathbf{q})|^2$ is presented as a function of the phonon momentum **q** at fixed values of the initial electron momentum **k**. The values of **k** were chosen according to ARPES data in which renormalization of the effective electron mass, which indicates interaction between electrons and collective excitations, was detected in the nodal direction for $\mathbf{k}_n = ((1-\delta)\pi/2; (1-\delta)\pi/2)$ and in the nodal direction for $\mathbf{k}_{\text{an}} = (\pi(1-\delta); \delta)$ (where $\delta \sim 0.1$). Figures 2–5 show maps for the diago-

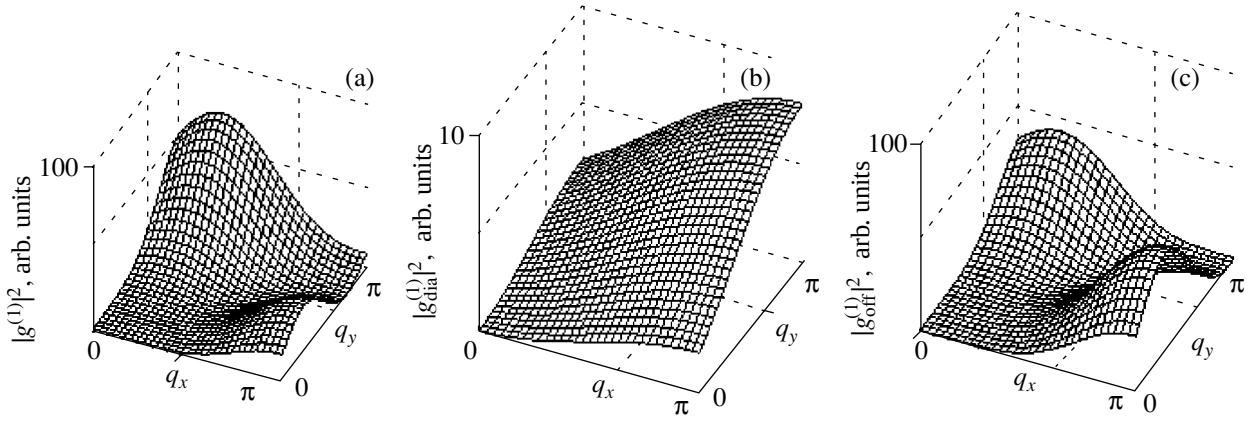

Fig. 3. EPI matrix element for the breathing mode at the $\mathbf{k}_{\rm an}$ antinodal point: (a) the total element, (b) the diagonal part, and (c) the off-diagonal part.

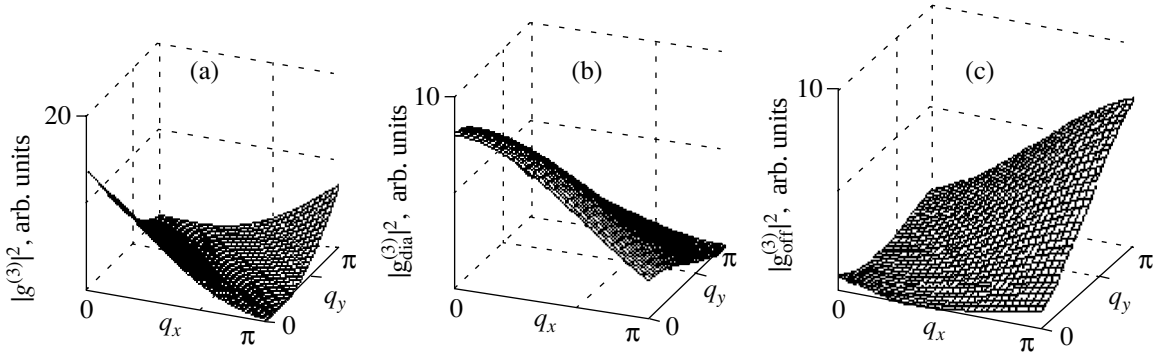

Fig. 4. EPI matrix element for the bending mode at the $\mathbf{k}_n$ nodal point: (a) the total element, (b) the diagonal part, and (c) the off-diagonal part.

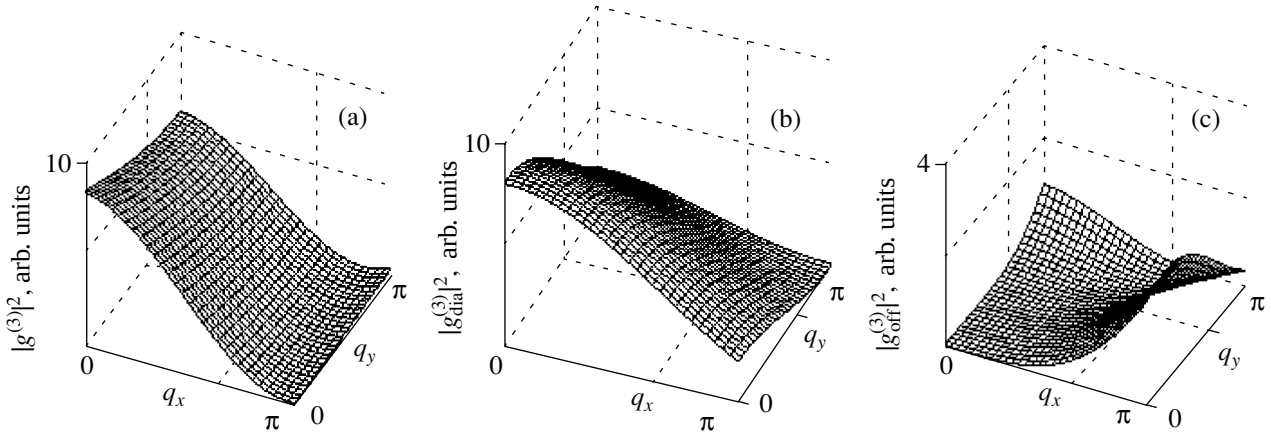

Fig. 5. EPI matrix element for the bending mode at the $\mathbf{k}_{\rm an}$ antinodal point: (a) the total element, (b) the diagonal part, and (c) the off-diagonal part.

nal and off-diagonal matrix elements for EPI with the breathing and bending modes at the nodal and antinodal points. All the maps were plotted for $\mathbf{g}^{(\nu)}_m = \mathbf{V}^{(\nu)}_{mm'} = 1$. The total intensity $|g^{(\nu)}_{{\rm dia},\,m}(\mathbf{q}) + g^{(\nu)}_{{\rm off},\,mm}(\mathbf{k}, \mathbf{q})|^2$ for quasiparticles that are diagonal in the band index m, $g^{(\nu)}_{mm}(\mathbf{k}, \mathbf{q})$ is characterized by interference of the $g_{\rm dia}$ and $g_{\rm off}$ matrix elements. An example of interference is shown in Fig. 2a for the breathing mode, where the peak height at $\mathbf{q} = (3\pi/4, 3\pi/4)$ in the total matrix ele-

ment is smaller than that in the partial $|g_{off}(\mathbf{k}, \mathbf{q})|^2$ contribution (Fig. 2c) for the same $\mathbf{q}$ point.

For the nodal $\mathbf{k}_n$ point, the $|g^{(1)}(\mathbf{k}_n, \mathbf{q})|^2$ maxima of the breathing mode (Fig. 2a) near the $\mathbf{q}$ points equal to $(3\pi/4; 3\pi/4)$, $(\pi; 0)$, and $(0; \pi)$ correspond to an off-diagonal contribution (Fig. 2c), and the diagonal part (Fig. 2b) causes a weak maximum at the $(\pi; \pi)$ point. (It is easy to see that the off-diagonal contribution for $\mathbf{q} = (\pi; \pi)$ becomes zero, just as in [23].) The maximum effective electron–phonon interaction is determined by vibrations with the wavevectors $\mathbf{q}$ located at the edges of the Brillouin zone. It is these phonons that transfer an electron from $\mathbf{k} \sim \mathbf{k}_F$ into states with the final momentum $\mathbf{k}' = \mathbf{k} + \mathbf{q}$ lying at the Fermi surface. The intensity of interaction with electrons for the half-breathing mode $\mathbf{q} = (\pi; 0)$ is higher than that for the full breathing mode $\mathbf{q} = (\pi; \pi)$. This finding agrees well with experiments. As was shown in inelastic neutron scattering experiments, the spectrum renormalization with doping for the $(\pi; 0)$ mode is about 20%, whereas it is only 5% for vibrations with the $(\pi; \pi)$ wavevector [30, 31]. Note that the softening and the line broadening and asymmetry of the half-breathing mode were detected in a number of HTSCs (e.g., in LSCO [32], YBCO [33], BKBO [34]). Moreover, the frequency of this vibration (70–85 meV) falls in the range of the kink energy in the nodal direction. The energy of the full breathing mode is 85–90 meV, which is higher than this value.

The interaction of the breathing mode with electrons having an initial momentum $\mathbf{k}_{an}$ is effectively small. The $|g^{(1)}(\mathbf{k}_{an}, \mathbf{q})|^2$ maximum at the $(0; \pi)$ point (Fig. 3a) corresponds to the scattering of electrons having an initial momentum $\mathbf{k}_{an}$ near the Fermi surface into the final state $\mathbf{k}' = \mathbf{k} + \mathbf{q} \approx (\pi; \pi)$, which is far from the Fermi surface. (Similar considerations are valid for the maximum at the $(\pi; 0)$ point). Note that the diagonal contribution at the maxima is small (Fig. 3b), and the off-diagonal contribution is the main contribution (Fig. 3c).

For the bending mode, the effective interaction is maximal at small values of the phonon momentum in both the nodal (Fig. 4) and antinodal (Fig. 5) directions. In both cases, the result depends on the diagonal contribution to the total matrix element.

For the apical breathing mode, electron–phonon interaction is independent of the $\mathbf{k}$ and $\mathbf{q}$ vectors.

Thus, an analysis of the atomic displacements of the vibrations under study shows the following. The interaction of electrons at the nodal point is maximal for the half-breathing mode with $\mathbf{q} = (\pi; 0)$ and for the bending mode with small values of the wavevector $\mathbf{q}$. The bending mode also strongly interact with electrons at the antinodal point at small values of $\mathbf{q}$. Moreover, the matrix element squared ($|g^{(1)}(\mathbf{k}, \mathbf{q})|^2$) for the half-breathing mode is higher than that for the full breathing mode $\mathbf{q} = (\pi; \pi)$ at any values of the initial electron momentum $\mathbf{k}$.

4. ELECTRON–PHONON INTERACTION IN AN EFFECTIVE LOW-ENERGY MODEL

Intersite hoppings in Hamiltonian (7) contain intraband hoppings in the lower Hubbard hole band ($m = 0$, the conduction band bottom in the electron representation) and in the upper Hubbard hole band ($m = 1$, the valence band top). The corresponding Hubbard operators are $X_f^0 \equiv X_f^{0\sigma}$ and $X_f^1 \equiv X_f^{-\sigma S}$.

Moreover, there are interband hoppings with excitation through a gap with charge transfer Δ that are described by the terms

$$t_{fg}^{01} X_f^{\dagger 0} X_g^1 = t_{fg}^{01} X_f^{\sigma 0} X_f^{-\sigma S}. \tag{27}$$

The elimination of the interband hoppings result in the effective low-energy one-band t–J_* model [35]; for the lower Hubbard band (electron doping), it can be written in the form

$$H_{t-J_*} = H_{t-J} + H_{(3)},$$

$$H_{t-J} = \sum_{f\sigma} \varepsilon_1 X_f^{\sigma\sigma} + \sum_{fg\sigma} t_{fg}^{00} X_f^{\sigma 0} X_g^{0\sigma} + \sum_{fg} J_{fg}\left(\mathbf{S}_f \cdot \mathbf{S}_g - \frac{1}{4} n_f n_g\right), \tag{28}$$

$$H_{(3)} = \sum_{fgm\sigma} \frac{t_{fm}^{01} t_{mg}^{01}}{\Delta} (X_f^{\sigma 0} X_m^{\bar\sigma\bar\sigma} X_g^{0\sigma} - X_f^{\sigma 0} X_m^{\bar\sigma\sigma} X_g^{0\bar\sigma}).$$

Here, $J_{fg} = 2(t_{fg}^{01})^2/\Delta$ is the exchange integral; $\mathbf{S}_f$ and n_f are the spin operator and the operator of the number of particles at the site; and $\bar\sigma = -\sigma$.

Off-diagonal EPI processes in Hamiltonian (10) contain intraband processes of the form

$$\mathbf{V}^{01} \mathbf{u}_{fg} X_f^{\sigma 0} X_g^{\bar\sigma S}. \tag{29}$$

Their elimination in the second order in $\mathbf{V}^{01}$ corresponds to the corrections $\delta J_{fg} \sim (\mathbf{V}^{01})^2 \mathbf{u}_{fg}^2/\Delta$ to the exchange integral, and we neglect them, since we restrict ourselves to linear-in-displacement contributions. At the same time, a combination of two perturbations (27) and (29) gives a linear-in-displacement correction to the exchange integral (spin–phonon interaction):

$$\delta J_{fg} = \frac{2 t_{fg}^{01} \mathbf{V}^{01} \cdot \mathbf{u}_{fg}}{\Delta} = \frac{\mathbf{V}^{01} \cdot \mathbf{u}_{fg}}{t_{fg}^{01}} J_{fg}. \tag{30}$$

Since the displacements are small and since $\mathbf{V}^{01}\mathbf{u} \ll t^{01}$ in series (9), we have $\delta J \ll J$. The spin–phonon interac-

tion Hamiltonian is

$$H_{\text{s-ph}} = \sum_{fg\mathbf{q}\nu} A_{fg}(\mathbf{q}, \nu)\left(\mathbf{S}_f \cdot \mathbf{S}_g - \frac{1}{4} n_f n_g\right) \times (b_{\mathbf{q},\nu} + b^{\dagger}_{-\mathbf{q},\nu}),$$
$$A_{fg}(\mathbf{q}, \nu) = \frac{2it^{01}_{fg}/\Delta}{\sqrt{2M_0\omega_{\mathbf{q},\nu}}} e^{i\mathbf{q}\cdot(\mathbf{R}_f + \mathbf{R}_g)} \times (\mathbf{V}^{(\nu)}_{01,x}\delta_{f,g\pm x} + \mathbf{V}^{(\nu)}_{01,y}\delta_{f,g\pm y}). \quad (31)$$

Analogous linear-in-displacement corrections also appear in the three-center terms:

$$H^{(3)}_{\text{el-ph}} = -\sum_{fgm\sigma} \frac{\mathbf{V}^{01}(t_{fm}\mathbf{u}_{mg} + \mathbf{u}_{fm}t_{mg})}{\Delta} \times (X^{\sigma 0}_f X^{\bar{\sigma}\bar{\sigma}}_m X^{0\sigma}_g - X^{\sigma 0}_f X^{\bar{\sigma}\sigma}_m X^{0\bar{\sigma}}_g). \quad (32)$$

In (30) and (32), we ignore the corrections that are linear in displacements but small in the $\mathbf{V}^{01} \cdot \mathbf{u}/\Delta$ parameter.

Thus, by making allowance for electron–phonon interaction, we can write the effective low-energy *t–J** model as follows:

$$H_{\text{eff}} = H_{t-J^*} + H^0_{\text{ph}} + H_{\text{el-ph}} + H_{\text{s-ph}} + H^{(3)}_{\text{el-ph}},$$
$$H^0_{\text{ph}} = \sum_{\mathbf{q}\nu} \omega_{\mathbf{q},\nu} b^{\dagger}_{\mathbf{q},\nu} b_{\mathbf{q},\nu}, \quad (33)$$
$$H_{\text{el-ph}} = \sum_{k\mathbf{q}\nu\sigma} g^{(\nu)}_{00}(\mathbf{q}, \nu) X^{\sigma 0}_{\mathbf{k}+\mathbf{q}} X^{0\sigma}_{\mathbf{k}} (b_{\mathbf{q},\nu} + b^{\dagger}_{-\mathbf{q},\nu}).$$

The band structure of the *p*-type cuprates is formed with the participation of two-particle $^1A_1$ singlet and $^3B_1$ triplet and is more complex [12]; however, the contribution of the triplet band Ω_T to the dispersion and the density of states manifests itself mainly below (by 0.5 eV) the valence band top, near which the Fermi level is pinned upon doping up to an optimum concentration ($x \le x_{\text{opt}}$). Therefore, to discuss the kinks and superconducting mechanisms, we may neglect the triplet band; then, we obtain an effective hole Hamiltonian that is identical to Hamiltonian (33) in which the operator $X^{0\sigma}$ of the lower Hubbard hole band is replaced by the operator $X^{\bar{\sigma}2}$ of the upper band ($m = 0 \longrightarrow m = 1$).

We now consider the simplest EPI contribution to the electron mass operator,

$$\Sigma(\mathbf{k}, \varepsilon) = \frac{1}{N}\sum_{\mathbf{q}\nu}\int d\omega \left|g^{(\nu)}_{00}(\mathbf{q}, \mathbf{k})\right|^2 \times G(\mathbf{k}-\mathbf{q}, \varepsilon-\omega) D(\mathbf{q}, \omega). \quad (34)$$

Detailed computation of spectrum renormalizations is beyond the scope of this work, and we only present qualitative notes. First, electrons in the strong-correlation regime in the *t–J* model are described as quasiparticles in the Hubbard subband, and their spectral weight is specified by the filling factor F_m in the numerator of the Green function (see Eq. (3)). For electron doping in $Nd_{2-x}Ce_xCuO_4$, we have

$$F_0 = \langle X^{00}\rangle + \langle X^{\sigma\sigma}\rangle = (1 + x)/2,$$

and for hole doping in $La_{2-x}Sr_xCuO_4$ we have

$$F_1 = \langle X^{\sigma\sigma}\rangle + \langle X^{S,S}\rangle = (1 + x)/2.$$

This spectral weight of quasiparticles appears in the Hartree–Fock Green function *G* in Eq. (34); as a result, the dimensionless EPI parameter for free electrons, $\lambda_0 = (g^2/\omega_D)N(0)$, decreases by the filling factor: $\lambda = \lambda_0(1 + x)/2$.

Second, based on EPI intensity maps and on the energy and momentum conservation laws, we can qualitatively analyze the modes that contribute to the kinks. In this analysis, we assume that the electron energy in the superconducting phase is described by the Bardeen–Cooper–Schrieffer formula

$$E(k) = \pm\sqrt{\varepsilon_k^2 + \Delta_k^2},$$

the Δ_k gap has the $d_{x^2-y^2}$ symmetry, and $\Delta(\mathbf{k}) = \Delta_0(\cos k_x a - \cos k_y a)/2$.

We now consider $\Sigma(\mathbf{k}, \varepsilon)$ at the nodal point $\mathbf{k}_n = ((1 - \delta)\pi/2; (1 - \delta)\pi/2)$, $\delta \le 0.1$. For the breathing mode, we have interaction maxima with transferred momenta $\mathbf{q}_1 = (3\pi/4; 3\pi/4)$ and $\mathbf{q}_2 = (\pi; \pi)$ (Fig. 2). An electron with $\mathbf{k}_n - \mathbf{q}_1$ is far from the Fermi surface, and the state with $\mathbf{k}_n - \mathbf{q}_2$ is near the Fermi level. Here, $E(\mathbf{k}_n - \mathbf{q}_2) \approx \Delta(\mathbf{k}_n - \mathbf{q}_2) = 0$ both above and below T_c; therefore, for a kink energy $\varepsilon(\mathbf{k}_n) = |E(\mathbf{k}_n - \mathbf{q}) - \omega^{(1)}_{\mathbf{q}}|$, we obtain $\varepsilon(\mathbf{k}_n) = 70$ meV, which corresponds to the breathing-mode energy. An EPI maximum at the point $\mathbf{q}_3 = (\pi; 0)$ (the half-breathing mode) is also visible in Fig. 2. The vector $\mathbf{k}_n - \mathbf{q}_3 \approx (-\pi/2; \pi/2)$ is close to the nodal point; therefore, this mode obeys the energy conservation law. For the bending mode with an energy $\omega \approx 35$ meV, EPI maxima are at the points $\mathbf{q} = (0; 0)$ and $\mathbf{q} = (\pi; \pi)$ (Fig. 4) and the vectors $\mathbf{k}_n - \mathbf{q}$ are close to $\mathbf{k}_n$; however, the energy conservation law with $\varepsilon(\mathbf{k}_n) = 70$ meV does not hold true. Thus, contributions to the electronic-spectrum renormalizations at the nodal point are caused by diagonal EPI with the breathing mode and by off-diagonal EPI with the half-breathing mode, with the kink energy being temperature-independent because of the gap symmetry $\Delta(\mathbf{k})$.

Similarly, for the antinodal point $\mathbf{k}_{\text{an}}$, EPI with the breathing mode has maxima for $\mathbf{q}_2 = (\pi; \pi)$ (from a diagonal matrix element) and for $\mathbf{q}_3 = (\pi; 0)$ (from an

off-diagonal matrix element) (Fig. 3). The state with $\mathbf{k}_{an} - \mathbf{q}_2$ is close to the antinodal point and $E(\mathbf{k}_{an} - \mathbf{q}_2) \approx \Delta(\pi; 0) \sim \Delta_0 \approx 35$ meV (this is true of optimally doped Bi2212, where kinks with energies of 40 meV at T = 100 K and of 70 meV at T = 10 K were detected [4]). The state with $\mathbf{k}_{an} - \mathbf{q}_3$ lies far from the Fermi surface and is of little interest. The contribution from the breathing mode does not obey the energy conservation law at both $T > T_c$ and $T < T_c$. However, EPI with the bending mode at $q = 0$ obeys all conservation laws (Fig. 5). At $T < T_c$, we have

$$\varepsilon(\mathbf{k}_{an}) = 70 \approx \left|\Delta_0 + \omega_{\mathbf{q}}^{(3)}\right|,$$

and at $T > T_c$ we have

$$\varepsilon(\mathbf{k}_{an}) \approx \omega_{\mathbf{q}}^{(3)}.$$

According to [4], a sharp decrease in the kink amplitude at the antinodal point above T_c is caused by two factors: a decrease in the density of states at ε_F in the normal phase as compared to the superconducting phase and temperature-induced smearing. Thus, as in [4], we arrive at the conclusion that the kink at the antinodal point is mainly contributed by the bending mode.

5. DISCUSSION

The consideration of EPI given above implied the $La_{2-x}Sr_xCuO_4$ structure (the T structure). Let us qualitatively discuss changes in the EPI when going to the $Nd_{2-x}Ce_xCuO_4$ structure (the T' structure). The T' structure has no apical oxygen above and below the Cu ions; therefore, the main change is caused by the absence of the apical breathing mode with a strong EPI ($\nu = 2$ in our designations in Eq. (26)). Moreover, $g_{mm'}^{(3)}(\mathbf{k}, \mathbf{q})$ decreases substantially for EPI with the breathing mode, since the $\delta t'_{pp}$ and $\delta V'_{pp}$ contributions, which give linear-in-displacement terms in EPI for this mode (see discussion before Eq. (24)), disappear.

As for EPI with the breathing mode, the basic contribution is generated by oxygen-ion displacements in the Cu–O plane; therefore, we conclude that the values of $g_{mm'}^{(1)}(\mathbf{k}, \mathbf{q})$ for the T and T' structures differ only slightly. Inelastic neutron scattering experiments also indicate that the doping-induced changes in the phonon spectra of the breathing mode in $La_{2-x}Sr_xCuO_4$ and $Nd_{2-x}Ce_xCuO_4$ are similar [19]. A comparison of the EPIs in the T and T' structures makes it clear why the kink in the antinodal direction (0; 0)–(π; 0) is absent in $Nd_{2-x}Ce_xCuO_4$: it is absent because the interaction with the bending mode is smaller than that in $La_{2-x}Sr_xCuO_4$. If the EPI with the breathing mode changes only weakly, it is unclear why the kink in the nodal direction (0; 0)–(π; π) is absent. The ARPES data for $Nd_{2-x}Ce_xCuO_4$ in [36] imply weaker specific features in this direction.

To develop a superconducting theory, the effective Hamiltonian in which EPI is excluded using the Frolich transform is of interest [37]. Until we restrict ourselves to an effective Hamiltonian for the CuO_2 layer, the nonadiabatic effects caused by vibrations with wavevectors q_z along the c axis are insignificant [38]. For the t–J* model with phonons (33), the Fröhlich transform in terms of the X operators is nontrivial; therefore, we briefly dwell on it. We write a Hamiltonian as

$$H = H_{el} + H_{el-ph}, \tag{35}$$

where H_{el} is the Hamiltonian of the t–J* model (Eq. (33)) for the conduction band bottom ($m = 0$) or for the valence band top ($m = 1$) and H_{el-ph} is described by Eq. (26). In the canonical transformation $H_S = \exp(-S)H\exp(S)$, the S operator is chosen to be

$$S = \sum_{k\mathbf{q}\sigma}\sum_{mm'} (\alpha_{\mathbf{kq}}^{mm'} b_{-\mathbf{q}}^{\dagger} + \beta_{\mathbf{kq}}^{mm'} b_{\mathbf{q}}) X_{\mathbf{k}+\mathbf{q}}^{\dagger m} X_{\mathbf{k}}^{m'}. \tag{36}$$

As usual, we find the α and β coefficients from the condition

$$H_{el-ph} + [H_{el}, S] = 0 \tag{37}$$

and write H_{eff} as

$$H_S = H_{el} + \frac{1}{2}[H_{el-ph}, S]. \tag{38}$$

In solving Eq. (37), we neglect the interband contributions in Eq. (36). First, the EPI interband matrix elements are always smaller than the intraband elements, since the former elements only contain off-diagonal contributions (see Eq. (26)); second, interband excitations go through a large gap Δ between the lower and upper Hubbard subbands, so that the corresponding contributions are $\sim g_{mm'}^{(\nu)}/\Delta \ll 1$. In solving Eq. (37), we also use a Hubbard-I type approximation in the $[H_{el}, S]$ commutator. As a result, for the m band we obtain

$$\begin{aligned} \alpha_{\mathbf{kq},\nu}^{mm} &= g_{mm}^{(\nu)}(\mathbf{k}, \mathbf{q}) \\ &\times [(t_m(\mathbf{k}) - t_m(\mathbf{k}+\mathbf{q}))F_m - \omega_{\mathbf{q},\nu}]^{-1}, \\ \beta_{\mathbf{kq},\nu}^{mm} &= g_{mm}^{(\nu)}(k, q) \\ &\times [(t_m(\mathbf{k}) - t_m(\mathbf{k}+\mathbf{q}))F_m - \omega_{\mathbf{q},\nu}]^{-1}, \end{aligned} \tag{39}$$

where $t_m(\mathbf{k}) = \sum_k t_m(R)\exp(ikR)$. The dependence of α and β on the filling factor F_m and, hence, the dopant concentration appears as the effect of strong correlations. As a result, the effective Hamiltonian can be written as

$$H_{eff} = H_{t-J^*} + H_{el-ph-el}, \tag{40}$$

where H_{t-J^*} is described by Eq. (28) and $H_{\text{el–ph–el}}$ is defined as

$$H_{\text{el–ph–el}} = \sum_{\mathbf{k}\mathbf{k}'\mathbf{q}\nu}\sum_{m} V^{mm}_{\mathbf{k}\mathbf{k}'\mathbf{q}} X^{+m}_{\mathbf{k}+\mathbf{q}} X^{+m}_{\mathbf{k}'-\mathbf{q}} X^{m}_{\mathbf{k}'} X^{m}_{\mathbf{k}},$$

$$V^{mm}_{\mathbf{k}\mathbf{k}'\mathbf{q}} = g^{(\nu)}_{mm}(\mathbf{k}, \mathbf{q}) g^{(\nu)}_{mm}(\mathbf{k}', -q)\omega_{\mathbf{q},\nu} \quad (41)$$

$$\times [(t_m(\mathbf{k}) - t_m(\mathbf{k}+\mathbf{q}))^2 F_m^2 - w^2_{\mathbf{q},\nu}]^{-1}.$$

Here, $m = 0$ and $m = 1$ give effective Hamiltonians for the cuprates with electron and hole doping types, respectively.

In contrast to the analogous effective interaction of weakly correlated electrons, the effective interaction in the regime of strong electron correlations depends on the occupation numbers and, hence, on the concentration, temperature, and the magnetic field.

6. CONCLUSIONS

We have derived EPI within the framework of a multiband realistic model of cuprates in the regime of strong electron correlations. The number of different microscopic contributions is large, and they are caused by the modulation of all interatomic-distance-dependent parameters upon ionic displacements; these include one-electron parameters (t_{pd} and t_{pp} hoppings between various p and d orbitals and the one-electron energies of p and d orbitals in the crystal field) and two-electron parameters (Coulomb matrix elements). For each vibration mode ν, we combine different microscopic contributions to form two parameters that characterize diagonal EPI (on lattice sites) and off-diagonal EPI. Explicit dependences of the $g_{\text{dia}}(\mathbf{q})$ and $g_{\text{off}}(\mathbf{q})$ matrix elements on the wavevectors were found for three modes, namely, breathing, apical breathing, and bending modes. A symmetrical analysis of these matrix elements allowed the qualitative conclusion that EPI with the breathing mode is involved in the formation of a kink in an electronic spectrum in the nodal direction (0; 0)–(π; π) and that the bending mode is responsible for a kink in the antinodal direction (0; 0)–(π; 0).

It does not follow from our results that the kinks are only caused by EPI. We do not exclude additive EPI contributions and interaction with spin fluctuations. Note that the recent calculation [39] of electronic-spectrum renormalizations by the nonperturbation variational Monte Carlo method, which also includes interaction with spin fluctuations, has not revealed kinks and has detected weaker electronic-spectrum renormalizations.

A comparison of EPIs in the n-type cuprates with the T' lattice and in the p-type cuprates with the T lattice showed a weaker EPI in the T' lattice as compared to the T lattice. However, the EPIs for the breathing mode differ only weakly for these two types of cuprates. An additional origin of electron–hole asymmetry in the cuprates is related to different natures of the carrier bands: in the hole cuprates, carriers are holes moving along the oxygen p_σ orbitals, whereas in the electron cuprates carriers are predominantly electrons of the $d_{x^2-y^2}$ orbital of Cu.

The effects of strong correlations in EPI manifest themselves in the filling factors F_m, which are self-consistently determined via the occupation numbers of multielectron terms and are functions of the carrier concentration, the temperature, and the magnetic field. The same factors specify the nonintegral spectral weight of the Hubbard quasiparticles, i.e., the specific features of a band structure in strongly correlated systems.

ACKNOWLEDGMENTS

We thank E.G. Maksimov, V.V. Val'kov, and M.M. Korshunov for fruitful discussions.

This work was supported by the Russian Foundation for Basic Research (project no. 03-02-16124), the program "Quantum Macrophysics" of the Presidium of the Russian Academy of Sciences, the Foundation in Support for Russian Science, the Foundation of Noncommercial Programs Dynasty, and the International Center of Fundamental Physics in Moscow.

REFERENCES

1. E. G. Maksimov, Usp. Fiz. Nauk **170**, 1033 (2000) [Phys. Usp. **43**, 965 (2000)].
2. A. Damascelli, Z.-X. Shen, and Z. Hussain, Rev. Mod. Phys. **75**, 473 (2003).
3. A. D. Gromko, A. V. Fedorov, Y.-D. Chuang, *et al.*, Phys. Rev. B **68**, 174520 (2003).
4. T. Cuk, D. H. Lu, X. J. Zhou, *et al.*, Phys. Status Solidi B **242**, 11 (2005).
5. E. Schachinger, J. J. Tu, and J. P. Carbotte, Phys. Rev. B **67**, 214508 (2003).
6. A. Lanzara, P. V. Bogdanov, X. J. Zhou, *et al.*, Nature **412**, 510 (2001).
7. A. Kaminski, M. Randeria, J. C. Campuzano, *et al.*, Phys. Rev. Lett. **86**, 1070 (2001).
8. S. V. Borisenko, A. A. Kordyuk, T. K. Kimet, *et al.*, Phys. Rev. Lett. **90**, 207001 (2003).
9. T. M. Rice, Phys. Rev. B **41**, 7243 (1990).
10. V. I. Belinicher and A. L. Chernyshev, Phys. Rev. B **47**, 390 (1993).
11. M. L. Kulic and O. V. Dolgov, Phys. Status Solidi B **242**, 151 (2005).
12. V. A. Gavrichkov, S. G. Ovchinnikov, A. A. Borisov, and E. G. Goryachev, Zh. Éksp. Teor. Fiz. **118**, 422 (2000) [JETP **91**, 369 (2000)].
13. J. Song and J. F. Annett, Phys. Rev. B **51**, 3840 (1995).
14. R. Zeyer and M. L. Kulic, Phys. Rev. B **53**, 2850 (1996).

15. A. Nazarenko and E. Dagotto, Phys. Rev. B **53**, 2987 (1996).
16. T. Dahm, D. Manske, D. Fay, and L. Tewordt, Phys. Rev. B **54**, 12006 (1996).
17. N. Bulut and D. J. Scalapino, Phys. Rev. B **54**, 14971 (1996).
18. L. Pintschovius and M. Braden, Phys. Rev. B **60**, 15039 (1999).
19. L. Pintschovius, Phys. Status Solidi B **242**, 30 (2005).
20. T. S. Nunner, J. Schmailian, and K. N. Bennemann, Phys. Rev. B **59**, 8859 (1999).
21. T. P. Devereaux, T. Cuk, Z.-X. Shen, and N. Nagaosa, Phys. Rev. Lett. **93**, 117004 (2004).
22. O. Rösch and O. Gunnarsson, Phys. Rev. Lett. **92**, 146403 (2004).
23. S. Ishihara and N. Nagaosa, Phys. Rev. B **69**, 144520 (2004).
24. Yu. B. Gaididei and V. M. Loktev, Phys. Status Solidi B **147**, 307 (1988).
25. V. J. Emeri, Phys. Rev. Lett. **58**, 2794 (1987).
26. C. M. Varma, S. Schmitt-Rink, and E. Ebrahams, Solid State Commun. **62**, 681 (1987).
27. V. V. Val'kov and S. G. Ovchinnikov, *Quasi-particles in Strongly Correlated Systems* (Sib. Otd. Ross. Akad. Nauk, Novosibirsk, 2001) [in Russian].
28. M. M. Korshunov, V. A. Gavrichkov, S. G. Ovchinnikov, *et al.*, Zh. Éksp. Teor. Fiz. **126**, 642 (2004) [JETP **99**, 559 (2004)].
29. C. Falter, M. Klenner, and W. Ludwig, Phys. Rev. B **47**, 5390 (1993).
30. R. J. McQueeney, J. L. Sarrao, P. G. Pagliuso, *et al.*, Phys. Rev. Lett. **87**, 077001 (2001).
31. L. Pintschovious and M. Braden, Phys. Rev. B **60**, R15039 (1999).
32. L. Pintschovious, N. Pyka, W. Reichardtet, *et al.*, Physica C (Amsterdam) **185**–**189**, 156 (1991).
33. W. Reichardt, N. Pyka, L. Pintschovius, *et al.*, Physica C (Amsterdam) **162**–**164**, 464 (1989).
34. M. Braden, W. Reichardt, W. Schmidbauer, *et al.*, J. Supercond. **8**, 1 (1995).
35. L. N. Bulaevskiĭ, É. L. Nagaev, and D. I. Khomskiĭ, Zh. Éksp. Teor. Fiz. **54**, 1562 (1968) [Sov. Phys. JETP **27**, 836 (1968)].
36. N. P. Armitage, D. H. Lu, C. Kim, *et al.*, Phys. Rev. B **68**, 064517 (2003).
37. H. Fröhlich, Phys. Rev. **79**, 845 (1950).
38. C. Falter, Phys. Status Solidi B **242**, 78 (2005).
39. S. Yunoki, E. Dagotto, and S. Sorella, Phys. Rev. Lett. **94**, 037001 (2005).

Translated by K. Shakhlevich